Cell PRESS
Structure
Article

Structural Insights into Recognition of MDC1 by TopBP1 in DNA Replication Checkpoint Control

Charles Chung Yun Leung,[1] Luxin Sun,[1] Zihua Gong,[2] Michael Burkat,[1] Ross Edwards,[1] Mark Assmus,[1] Junjie Chen,[2] and J.N. Mark Glover[1,*]
[1]Department of Biochemistry, University of Alberta, Edmonton, Alberta T6G 2H7, Canada
[2]Department of Experimental Radiation Oncology, University of Texas M. D. Anderson Cancer Center, 1515 Holcombe Boulevard, Houston, TX 77030, USA
*Correspondence: mark.glover@ualberta.ca
http://dx.doi.org/10.1016/j.str.2013.06.015

SUMMARY

Activation of the DNA replication checkpoint by the ATR kinase requires protein interactions mediated by the ATR-activating protein, TopBP1. Accumulation of TopBP1 at stalled replication forks requires the interaction of TopBP1 BRCT5 with the phosphorylated SDT repeats of the adaptor protein MDC1. Here, we present the X-ray crystal structures of the tandem BRCT4/5 domains of TopBP1 free and in complex with a MDC1 consensus pSDpT phosphopeptide. TopBP1 BRCT4/5 adopts a variant BRCT-BRCT packing interface and recognizes its target peptide in a manner distinct from that observed in previous tandem BRCT- peptide structures. The phosphate-binding pocket and positively charged residues in a variant loop in BRCT5 present an extended binding surface for the negatively charged MDC1 phosphopeptide. Mutations in this surface reduce binding affinity and recruitment of TopBP1 to γH2AX foci in cells. These studies reveal a different mode of phosphopeptide binding by BRCT domains in the DNA damage response.

INTRODUCTION

The DNA replication checkpoint is crucial for the prevention of genomic instability during DNA replication in cells. Activation of the DNA replication checkpoint requires the orchestrated assembly of proteins at the stalled replication fork. Topoisomerase IIβ binding protein 1 (TopBP1) is key to the success of DNA replication checkpoint activation by operating at multiple and distinct steps that contribute to the robust activation of the critical Ser/Thr kinase, ataxia telangiectasia and Rad3 related (ATR). The abundance of conserved phosphopeptide binding BRCA1 C-terminal (BRCT) domains in TopBP1 provides extraordinary specificity to target different replication fork proteins. The TopBP1 N-terminal BRCT0/1/2 domains recognize the Rad9 C-terminal tail of the Rad9-Rad1-Hus1 (9-1-1) complex to activate ATR via the ATR activation domain (AAD) of TopBP1 (Delacroix et al., 2007; Lee et al., 2007). ATR kinase activity is further potentiated by a secondary interaction between the TopBP1 C-terminal BRCT7/8 domains and autophosphorylated ATR (Liu et al., 2011). In an earlier step in checkpoint activation, the TopBP1 BRCT7/8 domains bind BRCA1-associated C-terminal helicase/Fanconi anemia group J protein (BACH1/FANCJ) to regulate the helicase activity of BACH1 and increase single-stranded DNA and subsequent replication protein A loading (Gong et al., 2010). Despite these findings, it remained elusive how TopBP1 accumulates at stalled replication forks because TopBP1 localization is independent of BACH1 and Rad9 interactions (Gong et al., 2010; Yan and Michael, 2009).

We have shown that the fifth BRCT domain of TopBP1 is responsible for TopBP1 localization to stalled replication forks (Wang et al., 2011; Yamane et al., 2002). TopBP1 BRCT5 directly interacts with the phosphorylated Ser-Asp-Thr (SDT) repeats in mediator of DNA damage checkpoint protein 1 (MDC1), and this binding is required for sustaining and amplifying ATR activity for checkpoint activation (Wang et al., 2011). MDC1 is a critical DNA damage response (DDR) adaptor in DNA double-strand break (DSB) repair. The rapid phosphorylation of histone H2AX at Ser139 (γ-H2AX) by the Ser/Thr kinase ATM is recognized by the tandem BRCT domains of MDC1, which further functions as a platform to bind various DDR factors such as RNF8 and the MRE11-RAD50-NBS1 (MRN) complex (Huen and Chen, 2010). A region in MDC1 spanning amino acids 210–460 contains six highly conserved SDT motifs that are constitutively phosphorylated by casein kinase 2 (CK2). These diphosphorylated motifs are recognized by the FHA-BRCT-BRCT domain repeat in NBS1 (Chapman and Jackson, 2008; Melander et al., 2008; Spycher et al., 2008; Wu et al., 2008; Xu et al., 2008) and by the FHA domain of aprataxin (Becherel et al., 2010).

BRCT domains are versatile modules that form various domain assemblies and are implicated in numerous functions, including protein-protein, phosphopeptide, DNA, and poly(ADP-ribose) binding (Leung and Glover, 2011). The conserved mode of phosphopeptide recognition by tandem BRCT domains is well established through structural studies in DDR proteins such as BRCA1, MDC1, TopBP1, MCPH1, *S. pombe* Crb2, and *S. pombe* Brc1 (Clapperton et al., 2004; Kilkenny et al., 2008; Leung et al., 2011; Shiozaki et al., 2004; Singh et al., 2012; Stucki et al., 2005; Williams et al., 2004, 2010). The tandem BRCT presents an extended phosphopeptide binding surface, with a pSer/pThr binding pocket located at the N-terminal BRCT domain and a secondary pocket at the BRCT-BRCT interface with specificity for +3 or +3/+4 residues. Unlike conventional tandem BRCT domains that require both BRCT domains to

Table 1. Data Collection, Phasing, and Refinement Statistics

Data Collection	TopBP1 BRCT4/5	TopBP1 BRCT4/5-Peptide Complex
Space group	$P222_1$	$P1$
Cell dimensions		
a, b, c (Å)	35.90, 48.80, 126.09	58.81, 59.10, 78.31
α, β, γ (°)	90.00, 90.00, 90.00	102.05, 98.04, 114.34
Resolution (Å)	63.04–1.90	34.57–2.60
R_{sym}[a]	0.077 (0.497)	0.059 (0.402)
$I/\sigma I$	18.0 (2.5)	11.9 (2.2)
Completeness (%)	99.8 (99.2)	95.2 (95.2)
Redundancy	3.8 (3.7)	2.1 (2.1)
Refinement		
Resolution (Å)	38.60–1.90	34.57–2.60
No. reflections	18,137 (927)	26,637 (1,330)
R_{work}/R_{free}[b]	0.175/0.224	0.190/0.234
No. of atoms		
Protein	1,540	5,716
Peptide	–	159
Ligand	33	–
Water	238	257
Average B factor (Å^2)		
Protein	11.0	44.3
Peptide	–	58.6
Ligand	31.9	–
Water	23.7	33.6
Rmsd		
Bond lengths (Å)	0.011	0.009
Bond angles (°)	1.347	1.132

[a] $R_{sym} = \Sigma|I-\langle I\rangle|/\Sigma|I|$.
[b] $R = \Sigma||F_o|-|F_c||/\Sigma|F_o|$, R_{free} was calculated from 5% of the data excluded from refinement.

form a viable phosphopeptide binding surface, only the C-terminal BRCT5 of the tandem BRCT4/5 pair is needed for MDC1 interaction and indeed BRCT4 lacks key amino acids required for phosphopeptide recognition (Rappas et al., 2011). In light of this knowledge, we sought to delineate the molecular basis of TopBP1-MDC1 interaction by characterizing, both structurally and functionally, the interaction between the tandem TopBP1 BRCT4/5 domains and a MDC1 diphosphopeptide containing a consensus sequence of the SDT repeats. We show that TopBP1 BRCT4/5 adopts an unconventional tandem BRCT repeat structure with a phosphate-binding pocket in the C-terminal BRCT5 domain. The combination of the phosphate-binding pocket and a structured loop in BRCT5 creates an extended positively charged surface that mediates MDC1 SDT diphosphopeptide binding and TopBP1 accumulation to stalled replication forks.

RESULTS

Crystal Structure of TopBP1 BRCT4/5

The crystal structure of TopBP1 BRCT4/5 was solved to 1.9 Å resolution (Table 1). The tandem BRCT pair adopts a distinct domain packing, where the juxtaposition of the two BRCT domains is head-to-head (where head is defined as the α_1-α_3 face and tail as the α_2 face) rather than the head-to-tail arrangement characteristic of canonical BRCT repeats (Figure S1A available online). This is likely driven by a combination of the variant BRCT fold in the N-terminal BRCT4 and a significantly shorter linker region between BRCT4 and BRCT5 (Figure 1A; Figure S1B). TopBP1 BRCT4 lacks an α_2 helix, which in canonical BRCT repeats houses conserved residues that participate in phosphate binding and the hydrophobic BRCT-BRCT interface. Instead, the BRCT4 α_2 is replaced by a short loop that is solvent exposed rather than being involved at the BRCT-BRCT interface. A short linker helix (α_L) composed of three residues (Pro632, Leu633, and Phe634) is also part of a significantly shorter inter-BRCT linker in TopBP1 BRCT4/5 (Figure 1A). The inter-BRCT linker packs tightly between the adjacent BRCT domains to stabilize the BRCT-BRCT interface.

Because of the unusual head-to-head domain arrangement, the composition of the N-terminal domain face that contacts the C-terminal domain is significantly different from the one used in conventional BRCT repeats. The N-terminal domain face consists of residues from α_3 (Val617 and Thr618), the β_3-β_4 loop (Leu598 and Leu599), and linker region (Pro632, Leu633, Val637, Pro638, and Val639; Figure 1B, left). Contributions from these different regions substitute for the α_2 helix typically used in the canonical interface. Conversely, the C-terminal domain face that contacts the N-terminal domain involves the α_1' and α_3' helices, which are the same secondary structure elements used in canonical BRCT repeats. Residues that form this hydrophobic face include Ala659, Ser663, Leu664, Phe666, Leu667, and Leu670 of α_1' and Ile718, Leu722, Ala725, and Arg726 of α_3' (Figure 1B, right). Together, the α_3, β_3-β_4 loop, linker region, α_1' and α_3' helices form an extensive hydrophobic interface that enables a head-to-head domain packing in TopBP1 BRCT4/5.

To date, the phosphate-binding pockets identified in canonical BRCT repeats are found in the N-terminal BRCT. This enables the characteristic specificity for the +3 residue in a targeted phosphopeptide through a secondary pocket formed at the BRCT-BRCT interface. Besides being positioned on the opposite side of the canonical phosphopeptide binding surface, the putative phosphate-binding pocket in BRCT4 is highly acidic, and conserved phosphate-binding residues are instead substituted with Leu561, Glu568, and Glu604 (Figure 1C, left). Strikingly, an intact phosphate-binding pocket containing the conserved Ser654, Lys661, and Lys704 residues is instead found in the C-terminal BRCT5 (Figure 1C, right). Although the presence of a C-terminal phosphate-binding pocket is perplexing in comparison to other BRCT repeats, the possibility for BRCT5 to recognize a phosphate supports previous findings that BRCT5 interacts with phospho-MDC1 to control the DNA replication checkpoint (Wang et al., 2011).

To probe for potential protein binding surfaces on TopBP1 BRCT4/5, we first examined the electrostatic potential surface of TopBP1 BRCT4/5. Although the BRCT repeat structure carries an overall negative charge, a highly positively charged surface is located in BRCT5 (Figure 1D, left). This region is rich in basic residues that extend from the putative phosphate-binding pocket (Lys661 and Lys704) to the extended β_2'-β_3' loop (Arg681,

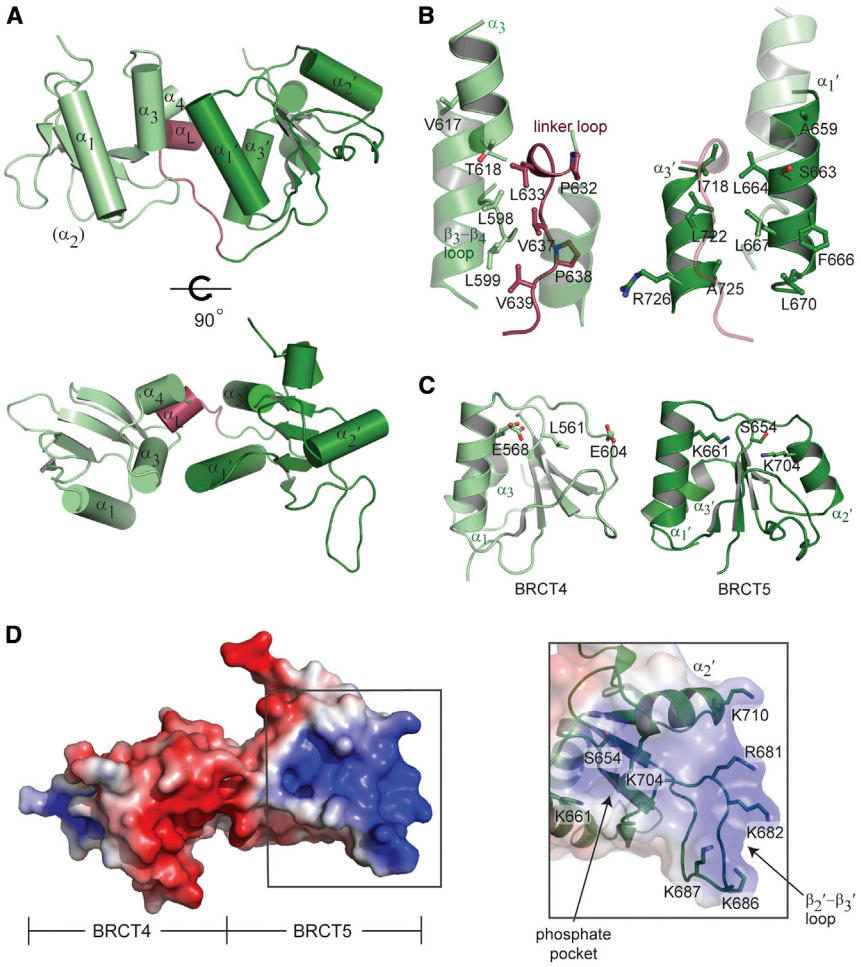

Figure 1. Crystal Structure of TopBP1 BRCT4/5

(A) Cartoon representation of TopBP1 BRCT4/5. BRCT4 (light green), BRCT5 (dark green), and the linker region (red) are colored accordingly. Secondary structure elements are labeled.

(B) BRCT-BRCT interface of TopBP1 BRCT4/5. Residues involved in the hydrophobic packing for the N-terminal face (left) and C-terminal face (right) are shown as sticks and labeled. The opposing interface is shown as transparent.

(C) Comparison of conserved phosphate-binding residues in BRCT4 (left) and BRCT5 (right).

(D) Electrostatic surface representation of TopBP1 BRCT4/5 oriented with BRCT4 on the left and BRCT5 on the right (left). The positively charged surface of BRCT5 is boxed. Residues that make up the BRCT5 phosphate-binding pocket and positively charged surface are shown as sticks and labeled (right).

See also Figure S1.

Lys682, Lys686, and Lys687) and C terminus of α_2' (Lys710; Figure 1D, right). Alignments of various tandem BRCT domains indicate that the β_2'-β_3' loop is the most variable region in the BRCT family (Glover et al., 2004). In TopBP1 BRCT5, the β_2'-β_3' loop adopts an unusually extended, structured protrusion. A series of main chain hydrogen bonds mediated by Asn684, Ala685, Lys687, Gly688, Met689, and Ala691 ensure rigidity of the loop (Figure S1C). The side chains of Asn684 and Ser683 also participate in hydrogen bonds with the loop main chain. This provides a structural platform for the four basic loop residues (Arg681, Lys682, Lys686, and Lys687) to create a positively charged concave pocket. Furthermore, the loop residues, especially Asn684 and the group of basic residues, are conserved in other species (Figure S1D).

TopBP1 BRCT4/5 Binds Phosphorylated MDC1 SDT Repeats

We have previously shown that TopBP1 BRCT5 interacts with a MDC1 diphosphopeptide encoding a consensus sequence of the six SDT repeats (Figure S2A; Wang et al., 2011). To further characterize binding specificities of this interaction in vitro, we used a fluorescence polarization (FP) assay. Using this assay, we tested for the ability of GST fusion proteins of TopBP1 BRCT5 and BRCT4/5 to bind a FITC-labeled MDC1 consensus SDT diphosphopeptide (GFIDpSDpTD VEEE). GST-BRCT4/5 and GST-BRCT5 bound the phosphopeptide with essentially identical affinities (K_d = 28 ± 4 μM for GST-BRCT5, K_d = 27 ± 4 μM for GST-BRCT4/5), indicating that BRCT4 is not important for the MDC1 interaction (Figure 2A, upper; Table 2). We next tested the importance of Ser/Thr phosphorylation for TopBP1 binding. A nonphosphorylated version of the SDT peptide bound TopBP1 BRCT5, albeit with a significant (~11-fold) reduction in binding affinity (Figure 2A, lower; Table 2). We also compared the affinity of TopBP1 BRCT5 affinity for doubly phosphorylated MDC1 peptides with MDC1 peptides bearing a single phosphate at either the Ser or Thr positions. The results indicate that either singly phosphorylated peptide is bound with a somewhat reduced (~3.5-fold) affinity compared to the doubly phosphorylated version (Figure 2A, lower; Table 2). This result indicates that both residues play a role in TopBP1 binding. The importance of phosphorylation for this interaction appears to be significantly less than that for other BRCT-phosphopeptide interactions. For example, TopBP1 BRCT7/8 binds its phosphorylated target peptide from BACH1 ~100-fold more tightly than the dephosphorylated peptide (Gong et al., 2010). This suggests that the mechanism of peptide recognition used by BRCT4/5 may be significantly different from that of other tandem BRCT repeats.

Crystal Structure of TopBP1 BRCT4/5 Bound to Phosphorylated MDC1

To further investigate the TopBP1-MDC1 interaction, we cocrystallized and solved the structure of TopBP1 BRCT4/5 in complex with a MDC1 diphosphopeptide to 2.6 Å resolution. A single MDC1 diphosphopeptide is bound in an extended conformation by two BRCT4/5 protomers on opposite sides (represented as protomers A and B, Figure 2B). The peptide-bound dimer is

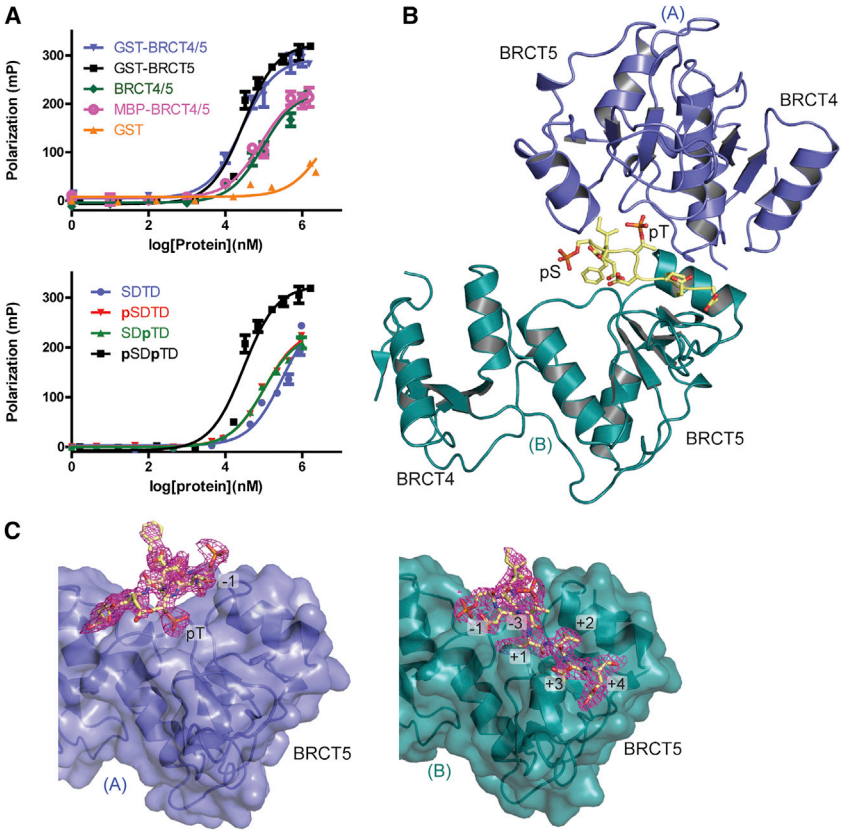

Figure 2. MDC1 SDT Diphosphopeptide Interactions with TopBP1 BRCT4/5

(A) FP binding results for the MDC1 FITC-labeled diphosphopeptide and various TopBP1 proteins. Triplicate data points are represented in graphs as mean ± SEM. (Top) FITC-peptide binding results for GST, GST-fusion proteins of BRCT4/5 and BRCT5, as well as untagged BRCT4/5 and MBP-BRCT4/5. (Bottom) FP assay of nonphosphorylated, pSer, pThr or diphosphorylated MDC1 FITC-labeled peptide with GST-TopBP1 BRCT5.

(B) Crystal structure of MDC1 diphosphopeptide in complex with TopBP1 BRCT4/5. The phosphorylated residues of the peptide (yellow) are labeled. BRCT4/5 protomer A (blue) and B (teal) are designated.

(C) Diphosphopeptide interactions with BRCT5 (represented in surface representation) of protomer A (left) and protomer B (right). The $2|F_o|-|F_c|$ electron density map for the diphosphopeptide is shown in magenta and peptide-interacting residues are labeled.

See also Figure S2.

further related by 2-fold noncrystallographic symmetry with another peptide-bound dimer in the asymmetric unit (Figure S2B). Comparisons of the apo and bound structures indicate that BRCT4/5 is structurally rigid and does not change significantly upon peptide binding (root-mean-square deviation [rmsd] for Cα = 0.39 and 0.46 with protomers A and B, respectively). The two protomers are oriented in an orthogonal manner in the dimer and interact indirectly through the MDC1 diphosphopeptide, except for a single hydrogen bond between the Tyr622 side chain of protomer A and the Gly702 main chain of protomer B. Consistent with previous data for BRCT5-mediated MDC1 binding, the MDC1 diphosphopeptide exclusively contacts the two BRCT5 domains from each protomer. Although the MDC1 diphosphopeptide interacts with two BRCT5 domains, their binding interfaces are not symmetrical and differ in size and composition. The majority of interactions with protomer A are contributed by the peptide pThr residue and bury a total solvent accessible surface area of 434 Å^2 (Figure 2C). This relatively small contact interface suggests that peptide interactions with protomer A are unlikely to be stable on its own and indeed some of the crystal contacts actually bury a larger surface area than the protomer A-peptide interface. In contrast, the interface between the diphosphopeptide and protomer B is more extensive, spanning residues −3 to +4 relative to the pThr and burying 919 Å^2 of solvent-accessible surface area (Figure 2C).

To test the possibility that two protomers of TopBP1 could bind to a MDC1 diphosphopeptide in solution, we assessed the impact of enforced dimerization on the peptide binding affinity of TopBP1. We compared the MDC1 diphosphopeptide binding affinities of GST-BRCT4/5 or GST-BRCT5, which both exist as dimers in solution, with monomeric forms of TopBP1 BRCT4/5 (Figure 2A, upper). The GST fusion-stabilized dimers bind MDC1 ~3-fold tighter than either the free BRCT4/5 or MBP-BRCT4/5, which are both monomeric as determined with gel filtration chromatography (K_d = 82 ± 16 μM for MBP-BRCT4/5; K_d = 94 ± 15 μM for untagged BRCT4/5). The enhanced affinity of the dimeric forms of TopBP1 over the monomeric forms is consistent with an avidity effect that would be expected in a structure where two protomers bind the MDC1 diphosphopeptide.

TopBP1 BRCT4/5-MDC1 SDT Repeat Binding Interactions

Unlike the highly specific phosphate-binding properties of canonical tandem BRCT domain pockets, peptide recognition by the BRCT5 phosphate-binding pocket relies more on general charge-charge interactions and water-mediated contacts. Interactions with BRCT5 of protomer A involve the MDC1 pThr and −1 Asp. The pThr is coordinated in the phosphate-binding pocket, but only participates in a single direct interaction with the conserved Lys704 side chain, although it makes water-mediated interactions with the main chain of Cys656 and Lys704 and side chain of Ser703 of protomer B (Figure 3A). Besides the pThr, the −1 Asp side chain also hydrogen bonds to the Ser703 main chain of protomer A. Unexpectedly, the −3 Asp, rather than the −2 pSer, points into the phosphate-binding pocket of protomer B (Figure 3B). The −2 pSer instead lies across the phosphate-binding pocket of protomer B. The −3 Asp side chain hydrogen bonds with the Gln655 main chain and Ser654 side chain, as well as the Lys704 side chain through a water molecule. Other contacts include a main chain–main chain hydrogen bond between the +1 Asp and Phe679 and

Table 2. Summary of Fluorescence Polarization Binding Experiments

Protein	Peptide	K_d (μM)
GST-BRCT5	FITC-GFID**SDTDV**EEE-NH2	310 ± 70
	FITC-GFID**pSDTDV**EEE-NH2	105 ± 9
	FITC-GFID**SDpTDV**EEE-NH2	98 ± 9
	FITC-GFID**pSDpTDV**EEE-NH2	28 ± 4
	FITC-GFID**pSDpTDD**EEE-NH2	24 ± 3
GST-BRCT4/5	FITC-GFID**pSDpTDV**EEE-NH2	27 ± 4
MBP-BRCT4/5	FITC-GFID**pSDpTDV**EEE-NH2	82 ± 16
BRCT4/5	FITC-GFID**pSDpTDV**EEE-NH2	94 ± 15
GST	FITC-GFID**pSDpTDV**EEE-NH2	ND
GST-BRCT5 Mutants		
S654A	FITC-GFID**pSDpTDV**EEE-NH2	32 ± 3
R681E/K682E	FITC-GFID**pSDpTDV**EEE-NH2	280 ± 60
K704A	FITC-GFID**pSDpTDV**EEE-NH2	210 ± 50

ND, not determined.

water-bridged interactions involving the Tyr678 side chain and the −1 and +1 Asp side chains.

Perhaps the most extensive interaction surface involves the recognition of the C-terminal residues of the conserved MDC1 SDT motif. As part of the larger binding interface established by protomer B, the +2 to +4 residues are recognized by the BRCT5 basic surface that extends from the phosphate-binding pocket to the β_2'-β_3' loop. The +2 Val sits in a small hydrophobic pocket situated between the basic phosphate-binding pocket and β_2'-β_3' loop (Figure 3C). Residues that contribute to this pocket include Ala707 and Trp711 from α_2' and Phe679 from the β_2'-β_3' loop. The conserved +3 and +4 Glu residues are cradled in the positively charged β_2'-β_3' loop. The +3 main chain hydrogen bonds with the main chain of Phe679 and Arg681 (Figure 3B), while the +3 and +4 acidic side chains make electrostatic interactions with Lys687 and Lys682, respectively (Figure 3C). Overall, the makeup of the BRCT5 binding surface matches the conservation of a small hydrophobic residue at +2 and acidic residues at +3 and +4 positions of the MDC1 SDT repeats (Figure S2A). The interactions between both protomers and the MDC1 diphosphopeptide are summarized in Figure 3D.

To test the importance of the conserved hydrophobic Val residue at the peptide +2 position, we compared the binding affinity of the wild-type MDC1 phosphopeptide with that of a peptide in which the +2 Val is substituted with an Asp. While a Val is the most common residue at this position, one of the MDC1 SDT repeats harbors an Asp at this position. We reasoned that if interactions between the diphosphopeptide and BRCT5 are purely electrostatic, then an increase in the overall negative charge of the peptide should enhance binding affinity. If instead the hydrophobic interactions involving the +2 residue are critical, then the substitution should reduce binding affinity. We observe, however, that the substitution results in no significant change in binding affinity (Figure S3A; Table 2). This may indicate that the loss in hydrophobic interactions in the mutant is balanced by long-range electrostatic interactions between the substituted Asp and the surrounding positively charged surface of BRCT5 and indicates that each of the SDT repeats are equally capable of binding TopBP1. The results suggest that the pocket may function to restrict the +2 residue to either a small hydrophobic residue or an Asp.

Mutational Analysis of BRCT5 Binding Interface

Because TopBP1 BRCT5 facilitates TopBP1 localization at stalled replication forks, we first generated several mutants within the BRCT5 domain and tested their abilities to form hydroxyurea (HU)-induced foci in cells. Mutations in the putative phosphate-binding pocket (K704A) or in the β_2'-β_3' loop (R681E/K682E) abolished foci formation, supporting the requirement for the positively charged BRCT5 surface (Figure 4A). In contrast, the S654A mutation did not disrupt TopBP1 foci formation but did appear to give less intense foci compared to background nuclear fluorescence in these cells. This is in agreement with the observation that the conserved Ser654 in the BRCT5 phosphate-binding pocket does not appear to have a major role in binding the MDC1 diphosphopeptide in the crystal structure. In contrast, the analogous Ser/Thr is required for phosphopeptide binding in several conventional tandem BRCT domains such as BRCA1, MDC1, and TopBP1 BRCT7/8, highlighting the distinct mechanism of phosphopeptide recognition used by TopBP1 BRCT4/5 (Leung and Glover, 2011). We next performed FP studies on various BRCT5 mutants to test whether the conserved positively charged surface is responsible for interactions with MDC1 in vitro. Consistent with TopBP1 localization, mutations in either the putative phosphate-binding pocket (K704A) or β_2'-β_3' loop (R681E/K682E) in GST-fusion proteins of BRCT5 significantly reduced binding to the MDC1 diphosphopeptide compared with wild-type (K_d ~210 ± 50 μM for K704A, K_d ~280 ± 60 μM for R681E/K682E; Figure 4B). In contrast, the S654A mutant bound the MDC1 diphosphopeptide with an affinity very similar to wild-type (K_d = 32 ± 3 μM). Overall, the specificity for the MDC1 SDT motif correlates with our mutational analysis and provides a rationale for the unusually structured and positively charged β_2'-β_3' loop exclusive to TopBP1 BRCT5.

DISCUSSION

The recognition of MDC1 by TopBP1 is critical for DNA replication checkpoint control in response to replication stress. TopBP1 BRCT5 directly binds to the conserved SDT repeats of MDC1, and this interaction is necessary for sustaining and amplifying ATR activation. In the context of phosphopeptide recognition by BRCT domains, the interaction between TopBP1 BRCT5 and the MDC1 SDT motifs was intriguing for several reasons. As part of a tandem BRCT pair, the functional requirement for only the C-terminal BRCT5 domain suggested that TopBP1 BRCT4/5 does not follow the canonical BRCT repeat mode of recognition (Wang et al., 2011; Yamane et al., 2002). The MDC1 SDT repeats are established diphosphopeptide motifs that are also targets for the FHA domains of NBS1 and Aprataxin in DNA repair (Becherel et al., 2010; Chapman and Jackson, 2008; Melander et al., 2008; Spycher et al., 2008; Wu et al., 2008; Xu et al., 2008). Because BRCT domain phosphate-binding pockets can bind to both pSer and pThr peptides (Leung et al., 2011), TopBP1 BRCT5 could potentially recognize only the pSer, pThr, or even both phosphorylated residues. Here we present the molecular basis for TopBP1 BRCT5 recognition of

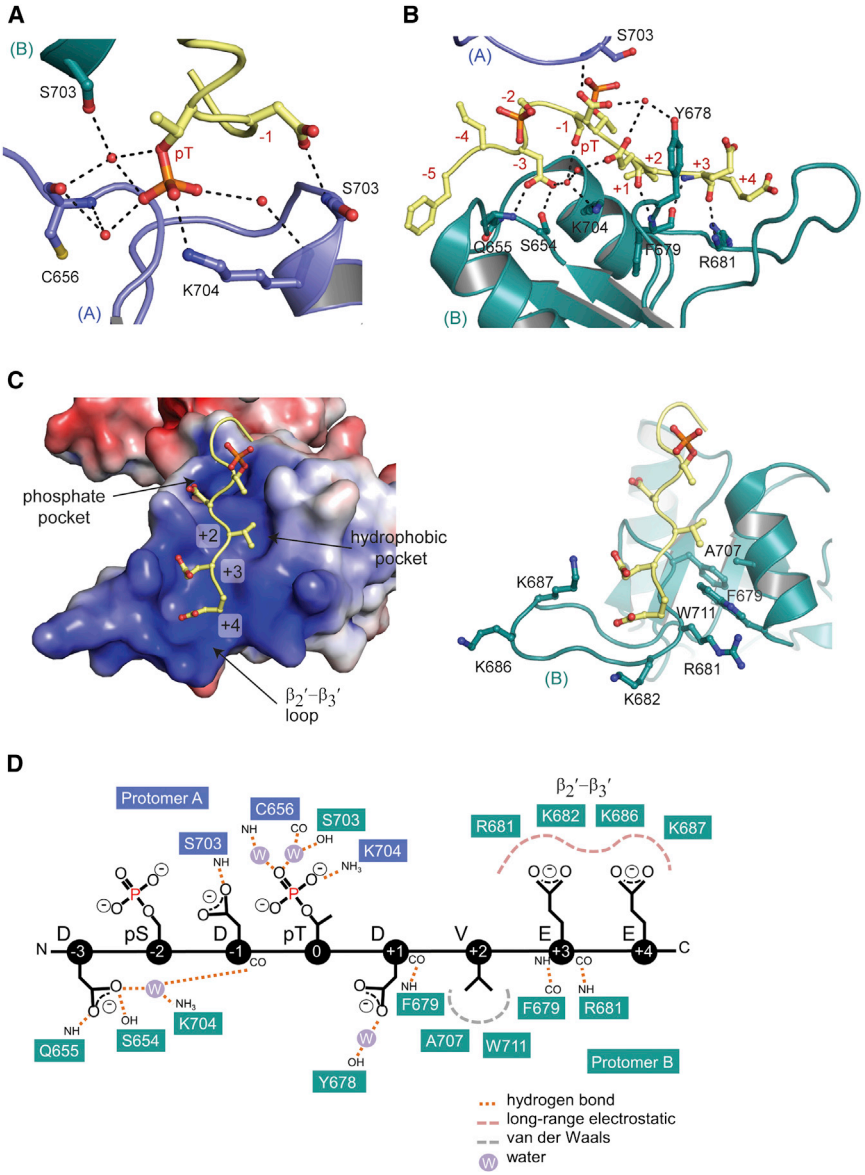

Figure 3. TopBP1 BRCT5 Diphosphopeptide Binding Interactions

(A) MDC1 peptide interactions with protomer A. Hydrogen bonding and electrostatic interactions are indicated by dotted lines and waters are shown as red spheres. Different TopBP1 protomers are designated as A and B.

(B) MDC1 peptide interactions with protomer B.

(C) Specificity of MDC1 peptide C-terminal residues by BRCT5 of protomer B in electrostatic surface representation (left) and cartoon (right).

(D) Schematic diagram of MDC1 peptide interactions with both TopBP1 BRCT5 protomers. See also Figure S3.

a MDC1 diphosphopeptide containing a consensus SDT repeat sequence. Our structural and functional analyses not only provide insight into the questions raised above, but also reveal other surprising aspects of BRCT phosphopeptide binding.

TopBP1 BRCT4/5 contains a number of structural features that diverges from a conventional BRCT repeat. An unexpected BRCT-BRCT packing interface results in a head-to-head arrangement of the BRCT domains. This is a consequence of an absent α_2-helix and constraints imposed by the relatively short inter-BRCT linker region. Rather than the α_2-α_1'-α_3' triple helix bundle associated with typical BRCT repeat interfaces, TopBP1 BRCT4/5 incorporates the same α_1'-α_3' helices from BRCT5 and a different surface composed of α_3 and the β_3-β_4 loop from BRCT4. Unconventional BRCT-BRCT interfaces have also been observed in the triple BRCT repeat, TopBP1 BRCT0/1/2, which coincidently also contains relatively shorter inter-BRCT linkers. However, the interfaces between BRCT0/1 and BRCT1/2 are distinct from BRCT4/5 and their respective C-terminal domain faces do not involve the α_1' and α_3' helices (Figure S1A; Rappas et al., 2011). Another difference is the presence of a phosphate-binding pocket in BRCT5 rather than the N-terminal BRCT4. Although this is rare in tandem BRCT domains, it is also found in the BRCT1/2 repeats in PAX-interacting protein 1 (PTIP) for example (Sheng et al., 2011). It is not clear, however, whether PTIP BRCT1/2 can bind phosphopeptides, and further structural and functional work will be needed to provide evidence for a common group of BRCT repeats that recognize phosphopeptides via a C-terminal BRCT pocket. Another possibility is that BRCT5 phosphopeptide recognition may in fact resemble phosphopeptide binding of single BRCT domains, a function that still remains unclear.

A striking feature of the peptide-bound structure is the lack of significant, tight contacts between either the pSer or pThr and the consensus phosphate-binding pocket of BRCT5. This is in contrast to all other structures of tandem BRCT domains bound to phosphopeptides where the phosphate is coordinated in a highly conserved manner (Leung and Glover, 2011). Indeed, FP results indicate that removal of both phosphate groups only results in an ~11-fold reduction in binding affinity, suggesting phosphorylation is less critical for TopBP1 BRCT4/5-phosphopeptide recognition than for other tandem BRCT-target phosphopeptide interactions. The lack of importance of the canonical phosphate-binding pocket is further underlined by the fact that mutation of the conserved Ser654 does not significantly impact phosphopeptide binding affinity or TopBP1 foci formation (Figure 4). This is in contrast with the analogous Ser1655 in the BRCA1 BRCT phosphate-binding pocket, which is critical for phosphopeptide binding and for BRCA1 BRCT domain function (Lee et al., 2010; Williams et al., 2004). Instead, phosphopeptide binding appears to largely rely on electrostatic interactions involving not only the phosphate-binding pocket, but also the extended

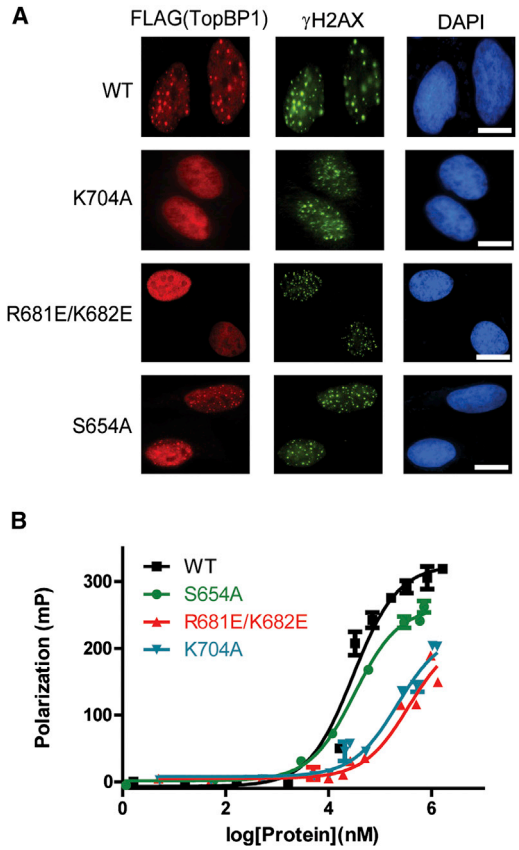

Figure 4. Mutational Analysis of the TopBP1 BRCT5 Binding Interface

(A) Replication stress-induced focus formation of wild-type and TopBP1 mutants. U2OS cells transfected with plasmids encoding SFB-tagged WT or mutants of TopBP1 were exposed to 2 mM HU for 3 hr. Cells were fixed and immunostained with anti-FLAG and anti-γ-H2AX antibodies. Bar: 10 μm.

(B) FP binding studies of MDC1 FITC-labeled diphosphopeptide with GST-fusion proteins of wild-type BRCT5 and various missense variants. Triplicate data points are represented in graphs as mean ± SEM.

β_2'-β_3' hairpin that contacts the conserved C-terminal acidic tail of the MDC1 phosphopeptide motif.

Perhaps the most surprising aspect of phosphopeptide recognition by TopBP1 BRCT5 is the apparent dimerization of BRCT5 induced by MDC1 binding. While the interface between protomer B and the phosphopeptide is quite large and specific mutations in its binding surface abrogate in vitro binding and foci formation, the interface with protomer A is much smaller and could be an artifact of crystal packing. We were unable to isolate or trap the peptide-induced dimer in solution using gel-filtration chromatography, chemical crosslinking, or EMSA. This would suggest either that the binding of two BRCT4/5 protomers to a single MDC1 diphosphopeptide does not occur in solution or that the interactions driving dimer formation with the phosphopeptide may be too transient to form a tight complex. On the other hand, we were able to demonstrate significantly higher MDC1 di-phospho-peptide binding affinities for dimeric GST-fusion proteins of BRCT4/5 than for monomeric MBP-BRCT4/5 or BRCT4/5 alone (Figure 2A). An explanation for this result could be that GST-induced dimerization indirectly stabilizes two BRCT4/5 domains in a state that favors the formation of the peptide-induced dimer observed in the crystal structure. If pairs of TopBP1 BRCT5 domains do bind phosphopeptide targets in the context of the intact full length protein, then this would imply that other regions in TopBP1 might be important to stabilize TopBP1 oligomerization. Indeed, TopBP1 has been shown to oligomerize through a tandem BRCT7/8-mediated recognition of an Akt-dependent internal TopBP1 pSer (pS1159) motif to stabilize the interaction between phospho-E2F1 and the single BRCT6 domain of TopBP1 (Liu et al., 2006). TopBP1 BRCT4/5 has also been shown to be important for the colocalization of TopBP1 with 53BP1 at DNA double strand breaks, where it may participate in the G1 DNA damage checkpoint (Cescutti et al., 2010). While the details of this interaction have not been elucidated, it is intriguing that colocalization and binding of the isolated BRCT4/5 with 53BP1 in cells appears to be dependent on ATM as well as fusion of the BRCT4/5 to a tetramerization domain. It is tempting to speculate that BRCT4/5 may bind one or more of the highly acidic ATM phosphorylation sites of 53BP1 (Jowsey et al., 2007) via a dimeric mechanism similar to that observed in the TopBP1 BRCT4/5-MDC1 complex.

The highly conserved MDC1 SDT repeats are not only recognized by TopBP1, but are also bound by the pThr-specific FHA binding domains of aprataxin and the FHA-tandem BRCT module of NBS1. Structural and biochemical studies of these interactions reveal a primary recognition of pThr within the FHA phosphate-binding pocket, with more limited electrostatic interactions involving the pSer as well as neighboring acidic residues in the pSDpT motif (Becherel et al., 2010; Lloyd et al., 2009; Williams et al., 2009). TopBP1 BRCT4/5, however, is distinct in its recognition of the conserved +2 to +4 residues. This suggests that the conservation of these residues in each of the SDT repeats in MDC1 is not solely for CK2 phosphorylation, but is also critical for TopBP1 binding. Clearly, further investigation is needed to understand how these diphosphopeptide motifs in MDC1 are recognized by a host of proteins in DDR.

Like the TopBP1-BACH1 interaction, the interaction between TopBP1 and MDC1 is also crucial for DNA replication checkpoint control. This study provides the structural basis that underlies another key TopBP1-mediated interaction that contributes to ATR activation and checkpoint signaling. Moreover, MDC1 binding by TopBP1 BRCT5 uncovers certain aspects of BRCT domain phosphopeptide recognition that further illustrate the diversity of BRCT domain function in the DNA damage response.

EXPERIMENTAL PROCEDURES

Cloning, Expression, and Purification

TopBP1 BRCT5 (641-746) was cloned into pGEX-4T-1 and BRCT4/5 (549–746) was cloned into pGEX-6P-1 (GE Healthcare) to create GST fusion proteins. BRCT4/5 (549–746) was cloned into pKM596 (New England Biolabs) to create an MBP fusion protein. BRCT5 mutants were engineered from BRCT5 (641–746) using PCR-directed overlap extension (Heckman and Pease, 2007) and cloned into pGEX-6P-1 vector. The GST fusion protein was expressed in *Escherichia coli* BL21-Gold cells and purified using glutathione affinity chromatography with glutathione sepharose 4B beads (GE Healthcare) and eluted in elution buffer (20 mM Tris-HCl pH 7.5, 150 mM NaCl, 20 mM reduced glutathione, and 0.1% BME). GST-fusion protein of BRCT5 was cleaved with thrombin protease (GE Healthcare) overnight at room temperature. BRCT5 was then separated from GST by cation

exchange chromatography (buffer A: 50 mM HEPES pH 7, and 0.1% BME; buffer B: 50 mM HEPES pH 7, 1 M NaCl, and 0.1% BME). BRCT5 was further purified on a Superdex 75 column in storage buffer (10 mM Tris-HCl pH 8, 150 mM NaCl, and 1 mM DTT). GST-TopBP1 BRCT4/5 was cleaved with PreScission protease overnight at 4°C. BRCT4/5 was purified by anion exchange chromatography (buffer A: 50 mM HEPES pH 7 and 0.1% BME; buffer B: 50 mM HEPES pH 7, 1 M NaCl, and 0.1% BME). Residual GST was removed by incubation with glutathione sepharose 4B beads (GE Healthcare) prior to a final purification step on a Superdex 75 column in storage buffer (10 mM Tris-HCl pH 7.5, 150 mM NaCl, and 1 mM DTT). The MBP-BRCT4/5 fusion protein was expressed in *E. coli* BL21-DE3 cells and purified using amylose affinity chromatography with amylose resin (New England Biolabs) and eluted in elution buffer (50 mM Tris-HCl pH 8, 150 mM NaCl, 10 mM Maltose, 1 mM EDTA, and 0.1% BME). MBP fusion protein was purified by anion exchange chromatography (buffer A: 50 mM HEPES pH 7, and 0.1% BME; buffer B: 50 mM HEPES pH 7, 1 M NaCl, and 0.1% BME) and further purified on a Superdex 75 column in storage buffer (10 mM Tris-HCl pH 7.5, 150 mM NaCl, and 1 mM DTT). The size and oligomeric state of each of the proteins was confirmed by size exclusion chromatography on a Superdex 75 column calibrated with protein size standards.

Crystallization

TopBP1 BRCT5 was concentrated to 9 mg/ml for crystallization. Crystals were grown at 4°C using hanging drop vapor diffusion by adding 2 μl protein with 1 μl reservoir consisting of 10% PEG 1000 and 0.1 M Na/K phosphate pH 6.2. Crystals were flash-cooled in cryoprotectant containing reservoir solution and 26% glycerol. TopBP1 BRCT4/5 was concentrated to 6.5 mg/ml for crystallization. Crystals were grown at room temperature in drops containing 1 μl protein and 1 μl reservoir (20% PEG 3350 and 0.2 M NaSCN). Cryoprotectant used to flash-cool crystals contained reservoir solution supplemented with 15% glycerol. For cocrystallization, TopBP1 BRCT4/5 concentrated to 12 mg/ml was incubated with a 1:6 molar ratio of protein:peptide (Ac-GFIDpSDpTDVEEE-NH_2) for 1 hr on ice. Cocrystals were grown at room temperature by adding 1 μl of protein:peptide mixture with 1 μl of reservoir solution containing 0.1 M ammonium acetate, 0.1 M bis-Tris pH 5.5and 17% PEG 10,000. Cocrystals were flash-cooled in reservoir solution supplemented with 20% glycerol.

Data Collection and Structure Determination

Data for BRCT5 and BRCT4/5 crystals were collected at the 8.3.1 beamline (Advanced Light Source, Berkeley). Intensity data from a BRCT5 crystal were processed using HKL2000 (Otwinowski and Minor, 1997) to the space group $P6_222$ with unit cell dimensions a = 91.00 Å, b = 91.00 Å, c = 114.31 Å, α = 90°, β = 90°, and γ = 120°. A starting model consisting of an ensemble of N-terminal BRCT domains (Protein Data Bank [PDB] IDs: 1JNX, 1R1Z, and 2ADO) was used in molecular replacement with PHASER (McCoy, 2007). The solution was then partially built in COOT (Emsley and Cowtan, 2004) and refined to 3.3 Å resolution with TLS and restrained refinement in REFMAC5 (Murshudov et al., 1997) to a R_{work} and R_{free} of 0.3887 and 0.4256, respectively. Data from a BRCT4/5 crystal were scaled and reduced to the space group $P222_1$ with unit cell dimensions a = 35.90 Å, b = 48.80 Å, c = 126.09 Å, α = 90°, β = 90°, and γ = 90°. The partially refined BRCT5 structure was used in molecular replacement to find one BRCT4/5 molecule in the asymmetric unit. Further refinement with rigid body and restrained refinement in REFMAC5 prior to automated model building using ARP/wARP (Cohen et al., 2008) successfully built 191 total residues with side chains. Further model building in COOT and refinement using PHENIX (Adams et al., 2010) at 1.9 Å resolution yielded a final R_{work} and R_{free} of 0.175 and 0.224, respectively. The final model lacks the N-terminal 549 residue and C-terminal 745–746 residues due to disorder in the crystal. The Ramachandran plot contains 100% of all residues in favored regions and 0% in outlier regions.

Data for crystals of the BRCT4/5-peptide complex were collected at the CMCF 08ID-1 beamline (Canadian Light Source, Saskatoon). Intensity data were scaled and reduced using the XDS package (Kabsch, 2010) to the space group *P1* with unit cell dimensions a = 58.81 Å, b = 59.10 Å, c = 78.31 Å, α = 102.05°, β = 98.04°, and γ = 114.34°. The apo BRCT4/5 structure was used in PHASER to successfully find 4 copies in the asymmetric unit. Model building was carried out in COOT and refined using TLS refinement (1 group/chain) and 2-fold NCS restraints in PHENIX. The BRCT4/5 molecules are arranged as two dimers (designated AB and CD) related by 2-fold noncrystallographic symmetry (Figure S2B). BRCT4/5 molecules A and C lack the N-terminal 549–550 residues, C-terminal 742–746 residues, and loop residues 584–588. Molecules B and D lack the N-terminal 549–550 residues, C-terminal 743–746 residues, and loop residues 584–589. The BRCT4/5 molecules were fully refined before building of the two peptides. Peptide A lacks the N-terminal −6 residue and C-terminal +5 residue and peptide B lacks the N-terminal −6 to −4 residues and C-terminal +5 residue (Figure S3B). Because there are slight deviations in the two peptide chain conformations (Figure S3C), 2-fold NCS restraints were not imposed for the peptide chains during refinement, which also yielded the lowest R_{free} statistics. The wxu_scale was set to 0.1 to reduce the X-ray/ADP weight. The final model was refined in Phenix at 2.6 Å resolution to a R_{work} and R_{free} of 0.190 and 0.234, respectively. The Ramachandran plot contained 96.8% of all residues in favored regions, 3.0% in allowed regions, and 0.3% in outlier regions.

Data collection and refinement statistics for the apo and peptide-bound structures are listed in Table 1. Models were validated with MolProbity (Chen et al., 2010). Secondary structure prediction of the models was performed with DSSP (Kabsch and Sander, 1983) and converted using DSSP2PDB (http://structure.usc.edu/dssp2pdb/). Hydrogen bonding was verified using HBPLUS (McDonald and Thornton, 1994). Structure figures were prepared with PyMOL (Version 1.4, Schrödinger).

Fluorescence Polarization

FP measurements were carried out using an Envision multi-label plate reader (Perkin Elmer) on a 384-well OptiPlate (Perkin Elmer). All peptides were synthesized and purified by Biomatik. FP assays were performed by mixing 10 nM FITC-labeled MDC1 phosphopeptide (FITC-GFIDpSDpTDVEEE-NH_2; FITC-GFIDpSDpTDDEEE-NH_2; FITC-GFIDSDpTDVEEE-NH_2; FITC-GFIDpSDTDVEEE-NH_2; FITC-GFIDSDTDVEEE-NH_2) with freshly concentrated TopBP1 in FP assay buffer (10 mM Tris-HCl pH 7.5, 150 mM NaCl, 1 mM DTT, and 0.05% Tween-20). The wells were incubated for 15 min at room temperature prior to taking FP measurements at an excitation wavelength of 485 nm and emission wavelength of 538 nm. Curve fitting and K_d calculations were obtained using PRISM software (GraphPad). K_d values presented in Table 2 are the averages from at least three independent titrations.

Immunofluorescence Staining

Cells grown on coverslips were treated with HU (2 mM) for 3 hr. Cells were fixed in 3% paraformaldehyde for 10 min, and then permeabilized in 0.5% Triton X-100 containing solution for 5 min. Cells were incubated with primary antibodies diluted in 5% goat serum at room temperature for 30 min. Cells were washed twice with PBS and then incubated with either FITC-conjugated or rhodamine-conjugated secondary antibodies at room temperature for 30 min. Nuclei were counterstained with DAPI. The coverslips were mounted onto glass slides with antifade solution and depicted using a Nikon Eclipse E800 fluorescence microscope with a 60 × NA 1.3 oil objective lens. Images were photographed and analyzed with a Spot 2 Megasample camera and Photoshop software (Adobe).

ACCESSION NUMBERS

The PDB accession codes for the coordinates for the TopBP1 BRCT4/5 (RCSB accession: 3UEN) and peptide-bound complex reported in this paper are 3UEN and 3UEO, respectively.

SUPPLEMENTAL INFORMATION

Supplemental Information includes three figures and can be found with this article online at http://dx.doi.org/10.1016/j.str.2013.06.015.

ACKNOWLEDGMENTS

We thank the staff at the ALS beamline 8.3.1, Dr. Pawel Grochulski, and the staff at the Canadian Light Source CMCF beamline 08ID-1 for assistance with synchrotron data collection. This work was supported by grants from

the Canadian Cancer Society (to J.N.M.G.) and the National Institutes of Health (CA92584 to J.N.M.G. and CA092312 to J.C.).

Received: January 10, 2013
Revised: June 14, 2013
Accepted: June 17, 2013
Published: July 25, 2013

REFERENCES

Adams, P.D., Afonine, P.V., Bunkóczi, G., Chen, V.B., Davis, I.W., Echols, N., Headd, J.J., Hung, L.W., Kapral, G.J., Grosse-Kunstleve, R.W., et al. (2010). PHENIX: a comprehensive Python-based system for macromolecular structure solution. Acta Crystallogr. D Biol. Crystallogr. *66*, 213–221.

Becherel, O.J., Jakob, B., Cherry, A.L., Gueven, N., Fusser, M., Kijas, A.W., Peng, C., Katyal, S., McKinnon, P.J., Chen, J., et al. (2010). CK2 phosphorylation-dependent interaction between aprataxin and MDC1 in the DNA damage response. Nucleic Acids Res. *38*, 1489–1503.

Cescutti, R., Negrini, S., Kohzaki, M., and Halazonetis, T.D. (2010). TopBP1 functions with 53BP1 in the G1 DNA damage checkpoint. EMBO J. *29*, 3723–3732.

Chapman, J.R., and Jackson, S.P. (2008). Phospho-dependent interactions between NBS1 and MDC1 mediate chromatin retention of the MRN complex at sites of DNA damage. EMBO Rep. *9*, 795–801.

Chen, V.B., Arendall, W.B., 3rd, Headd, J.J., Keedy, D.A., Immormino, R.M., Kapral, G.J., Murray, L.W., Richardson, J.S., and Richardson, D.C. (2010). MolProbity: all-atom structure validation for macromolecular crystallography. Acta Crystallogr. D Biol. Crystallogr. *66*, 12–21.

Clapperton, J.A., Manke, I.A., Lowery, D.M., Ho, T., Haire, L.F., Yaffe, M.B., and Smerdon, S.J. (2004). Structure and mechanism of BRCA1 BRCT domain recognition of phosphorylated BACH1 with implications for cancer. Nat. Struct. Mol. Biol. *11*, 512–518.

Cohen, S.X., Ben Jelloul, M., Long, F., Vagin, A., Knipscheer, P., Lebbink, J., Sixma, T.K., Lamzin, V.S., Murshudov, G.N., and Perrakis, A. (2008). ARP/wARP and molecular replacement: the next generation. Acta Crystallogr. D Biol. Crystallogr. *64*, 49–60.

Delacroix, S., Wagner, J.M., Kobayashi, M., Yamamoto, K., and Karnitz, L.M. (2007). The Rad9-Hus1-Rad1 (9-1-1) clamp activates checkpoint signaling via TopBP1. Genes Dev. *21*, 1472–1477.

Emsley, P., and Cowtan, K. (2004). Coot: model-building tools for molecular graphics. Acta Crystallogr. D Biol. Crystallogr. *60*, 2126–2132.

Glover, J.N., Williams, R.S., and Lee, M.S. (2004). Interactions between BRCT repeats and phosphoproteins: tangled up in two. Trends Biochem. Sci. *29*, 579–585.

Gong, Z., Kim, J.E., Leung, C.C., Glover, J.N., and Chen, J. (2010). BACH1/FANCJ acts with TopBP1 and participates early in DNA replication checkpoint control. Mol. Cell *37*, 438–446.

Heckman, K.L., and Pease, L.R. (2007). Gene splicing and mutagenesis by PCR-driven overlap extension. Nat. Protoc. *2*, 924–932.

Huen, M.S., and Chen, J. (2010). Assembly of checkpoint and repair machineries at DNA damage sites. Trends Biochem. Sci. *35*, 101–108.

Jowsey, P., Morrice, N.A., Hastie, C.J., McLauchlan, H., Toth, R., and Rouse, J. (2007). Characterisation of the sites of DNA damage-induced 53BP1 phosphorylation catalysed by ATM and ATR. DNA Repair (Amst.) *6*, 1536–1544.

Kabsch, W. (2010). Xds. Acta Crystallogr. D Biol. Crystallogr. *66*, 125–132.

Kabsch, W., and Sander, C. (1983). Dictionary of protein secondary structure: pattern recognition of hydrogen-bonded and geometrical features. Biopolymers *22*, 2577–2637.

Kilkenny, M.L., Doré, A.S., Roe, S.M., Nestoras, K., Ho, J.C., Watts, F.Z., and Pearl, L.H. (2008). Structural and functional analysis of the Crb2-BRCT2 domain reveals distinct roles in checkpoint signaling and DNA damage repair. Genes Dev. *22*, 2034–2047.

Lee, J., Kumagai, A., and Dunphy, W.G. (2007). The Rad9-Hus1-Rad1 checkpoint clamp regulates interaction of TopBP1 with ATR. J. Biol. Chem. *282*, 28036–28044.

Lee, M.S., Green, R., Marsillac, S.M., Coquelle, N., Williams, R.S., Yeung, T., Foo, D., Hau, D.D., Hui, B., Monteiro, A.N., and Glover, J.N. (2010). Comprehensive analysis of missense variations in the BRCT domain of BRCA1 by structural and functional assays. Cancer Res. *70*, 4880–4890.

Leung, C.C., and Glover, J.N. (2011). BRCT domains: easy as one, two, three. Cell Cycle *10*, 2461–2470.

Leung, C.C., Gong, Z., Chen, J., and Glover, J.N. (2011). Molecular basis of BACH1/FANCJ recognition by TopBP1 in DNA replication checkpoint control. J. Biol. Chem. *286*, 4292–4301.

Liu, K., Paik, J.C., Wang, B., Lin, F.T., and Lin, W.C. (2006). Regulation of TopBP1 oligomerization by Akt/PKB for cell survival. EMBO J. *25*, 4795–4807.

Liu, S., Shiotani, B., Lahiri, M., Maréchal, A., Tse, A., Leung, C.C., Glover, J.N., Yang, X.H., and Zou, L. (2011). ATR autophosphorylation as a molecular switch for checkpoint activation. Mol. Cell *43*, 192–202.

Lloyd, J., Chapman, J.R., Clapperton, J.A., Haire, L.F., Hartsuiker, E., Li, J., Carr, A.M., Jackson, S.P., and Smerdon, S.J. (2009). A supramodular FHA/BRCT-repeat architecture mediates Nbs1 adaptor function in response to DNA damage. Cell *139*, 100–111.

McCoy, A.J. (2007). Solving structures of protein complexes by molecular replacement with Phaser. Acta Crystallogr. D Biol. Crystallogr. *63*, 32–41.

McDonald, I.K., and Thornton, J.M. (1994). Satisfying hydrogen bonding potential in proteins. J. Mol. Biol. *238*, 777–793.

Melander, F., Bekker-Jensen, S., Falck, J., Bartek, J., Mailand, N., and Lukas, J. (2008). Phosphorylation of SDT repeats in the MDC1 N terminus triggers retention of NBS1 at the DNA damage-modified chromatin. J. Cell Biol. *181*, 213–226.

Murshudov, G.N., Vagin, A.A., and Dodson, E.J. (1997). Refinement of macromolecular structures by the maximum-likelihood method. Acta Crystallogr. D Biol. Crystallogr. *53*, 240–255.

Otwinowski, Z., and Minor, W. (1997). Processing of X-ray diffraction data collected in oscillation mode. Methods Enzymol. *276*, 307–326.

Rappas, M., Oliver, A.W., and Pearl, L.H. (2011). Structure and function of the Rad9-binding region of the DNA-damage checkpoint adaptor TopBP1. Nucleic Acids Res. *39*, 313–324.

Sheng, Z.Z., Zhao, Y.Q., and Huang, J.F. (2011). Functional evolution of BRCT domains from binding DNA to protein. Evol. Bioinform. Online *7*, 87–97.

Shiozaki, E.N., Gu, L., Yan, N., and Shi, Y. (2004). Structure of the BRCT repeats of BRCA1 bound to a BACH1 phosphopeptide: implications for signaling. Mol. Cell *14*, 405–412.

Singh, N., Basnet, H., Wiltshire, T.D., Mohammad, D.H., Thompson, J.R., Héroux, A., Botuyan, M.V., Yaffe, M.B., Couch, F.J., Rosenfeld, M.G., and Mer, G. (2012). Dual recognition of phosphoserine and phosphotyrosine in histone variant H2A.X by DNA damage response protein MCPH1. Proc. Natl. Acad. Sci. USA *109*, 14381–14386.

Spycher, C., Miller, E.S., Townsend, K., Pavic, L., Morrice, N.A., Janscak, P., Stewart, G.S., and Stucki, M. (2008). Constitutive phosphorylation of MDC1 physically links the MRE11-RAD50-NBS1 complex to damaged chromatin. J. Cell Biol. *181*, 227–240.

Stucki, M., Clapperton, J.A., Mohammad, D., Yaffe, M.B., Smerdon, S.J., and Jackson, S.P. (2005). MDC1 directly binds phosphorylated histone H2AX to regulate cellular responses to DNA double-strand breaks. Cell *123*, 1213–1226.

Wang, J., Gong, Z., and Chen, J. (2011). MDC1 collaborates with TopBP1 in DNA replication checkpoint control. J. Cell Biol. *193*, 267–273.

Williams, R.S., Lee, M.S., Hau, D.D., and Glover, J.N. (2004). Structural basis of phosphopeptide recognition by the BRCT domain of BRCA1. Nat. Struct. Mol. Biol. *11*, 519–525.

Williams, R.S., Dodson, G.E., Limbo, O., Yamada, Y., Williams, J.S., Guenther, G., Classen, S., Glover, J.N., Iwasaki, H., Russell, P., and Tainer, J.A. (2009). Nbs1 flexibly tethers Ctp1 and Mre11-Rad50 to coordinate DNA double-strand break processing and repair. Cell *139*, 87–99.

Williams, J.S., Williams, R.S., Dovey, C.L., Guenther, G., Tainer, J.A., and Russell, P. (2010). gammaH2A binds Brc1 to maintain genome integrity during S-phase. EMBO J. *29*, 1136–1148.

Wu, L., Luo, K., Lou, Z., and Chen, J. (2008). MDC1 regulates intra-S-phase checkpoint by targeting NBS1 to DNA double-strand breaks. Proc. Natl. Acad. Sci. USA *105*, 11200–11205.

Xu, C., Wu, L., Cui, G., Botuyan, M.V., Chen, J., and Mer, G. (2008). Structure of a second BRCT domain identified in the nijmegen breakage syndrome protein Nbs1 and its function in an MDC1-dependent localization of Nbs1 to DNA damage sites. J. Mol. Biol. *381*, 361–372.

Yamane, K., Wu, X., and Chen, J. (2002). A DNA damage-regulated BRCT-containing protein, TopBP1, is required for cell survival. Mol. Cell. Biol. *22*, 555–566.

Yan, S., and Michael, W.M. (2009). TopBP1 and DNA polymerase alpha-mediated recruitment of the 9-1-1 complex to stalled replication forks: implications for a replication restart-based mechanism for ATR checkpoint activation. Cell Cycle *8*, 2877–2884.

